Structural basis for iron piracy by pathogenic *Neisseria*

N. Noinaj[1], **N.C. Easley**[1], **M. Oke**[1], **N. Mizuno**[2], **J. Gumbart**[3], **E. Boura**[1], **A.N. Steere**[4], **O. Zak**[5], **P. Aisen**[5], **E. Tajkhorshid**[6], **R.W. Evans**[7], **A.R. Gorringe**[8], **A.B. Mason**[4], **A.C. Steven**[2], and **S.K. Buchanan**[1]

[1]Laboratory of Molecular Biology, National Institute of Diabetes and Digestive and Kidney Diseases, US National Institutes of Health, Bethesda, Maryland 20892

[2]Laboratory of Structural Biology, National Institute of Arthritis and Musculoskeletal and Skin Diseases, US National Institutes of Health, Bethesda, Maryland 20892

[3]Biosciences Division, Argonne National Laboratory, Argonne, Illinois 60439

[4]Department of Biochemistry, University of Vermont, College of Medicine, 89 Beaumont Avenue, Burlington, VT 05405 USA

[5]Albert Einstein College of Medicine, 1300 Morris Park Avenue, Bronx, NY 10461

[6]Department of Biochemistry and Beckman Institute, University of Illinois at Urbana-Champaign, Urbana, Illinois 61801

[7]Metalloprotein Research Group, Division of Biosciences, School of Health Sciences and Social Care, Brunel University, Uxbridge, Middlesex, UB8 3PH, UK

[8]Health Protection Agency, Porton Down, Salisbury SP2 8NY, UK

SUMMARY

Neisseria are obligate human pathogens causing bacterial meningitis, septicemia, and gonorrhea. *Neisseria* require iron for survival and can extract it directly from human transferrin for transport across the outer membrane. The transport system consists of TbpA, an integral outer membrane protein, and TbpB, a co-receptor attached to the cell surface; both proteins are potentially important vaccine and therapeutic targets. Two key questions driving *Neisseria* research are: 1) how human transferrin is specifically targeted, and 2) how the bacteria liberate iron from

transferrin at neutral pH. To address them, we solved crystal structures of the TbpA-transferrin complex and of the corresponding co-receptor TbpB. We characterized the TbpB-transferrin complex by small angle X-ray scattering and the TbpA-TbpB-transferrin complex by electron microscopy. Collectively, our studies provide a rational basis for the specificity of TbpA for human transferrin, show how TbpA promotes iron release from transferrin, and elucidate how TbpB facilitates this process.

INTRODUCTION

Neisseria comprise a large family of Gram-negative bacteria that colonize humans. Two family members, *N. gonorrhoeae* and *N. meningitidis,* are notorious pathogens that invade the urogenital tract and nasopharynx, respectively, causing gonorrhea, meningitis, and other systemic infections. Although vaccines exist for bacterial meningitis, they have significant limitations[1] and are ineffective against serogroup B *N. meningitidis.* Currently there are no vaccines to protect against gonococcal infections. The recent emergence of antibiotic resistant strains[2] adds urgency to the need to develop more effective countermeasures for both pathogens.

Neisseria require iron for survival and virulence[3]. Unlike most Gram-negative bacteria, *Neisseria* do not make siderophores but instead extract iron directly from serum transferrin in the human host (Tf). The Neisserial transport system consists of two large surface proteins: Tf binding protein A (TbpA), a 100 kDa integral outer membrane (OM) protein belonging to the family of TonB-dependent transporters[4] and Tf binding protein B (TbpB), an ~80 kDa co-receptor attached to the OM by a lipid anchor (Supplementary Fig. 1). Both proteins are found in all clinical isolates of pathogenic *Neisseria.* TbpA binds apo and iron-containing transferrin with similar affinities, whereas TbpB only associates with iron-bound Tf[5,6]. Although TbpA can extract and import iron without TbpB, the process is considerably more efficient in the presence of the co-receptor[7,8]. TbpA and TbpB induce bactericidal antibodies in mice against *N. meningitidis*[9,10] and *N. gonorrhoeae*[11], making both proteins important vaccine targets. In order to elucidate how TbpA and TbpB function to selectively bind human Tf and extract its tightly bound iron ($K_a=10^{23}$ M^{-1}) at physiological pH, we combined an approach consisting of X-ray crystallography, small angle X-ray scattering, and electron microscopy to determine a model of the 260 kDa iron import complex from *N. meningitidis* strain K454 (serogroup B). Because *N. gonorrhoeae* strains FA1090 and FA19 express TbpAs that are 94% identical to the meningococcal protein, while the corresponding TbpBs are 61% and 69% identical, respectively, our results are relevant to both pathogens.

RESULTS

Crystal structure of the TbpA-(apo)hTf complex

Structural characterization of the Neisserial iron import machinery was initiated by crystallizing *N. meningitidis* TbpA with full-length, glycosylated apo human transferrin (hTf) and solving the structure to a resolution of 2.6 Å (Fig. 1, Supplementary Fig. 2–4, 17, Supplementary Table 1). Despite being significantly larger (~20%) than other structurally characterized TonB-dependent transporters[4], TbpA retains the classic fold with a 22-strand

transmembrane β-barrel encompassing a plug domain (Fig. 1a). Most of the additional mass is found in several extracellular loops which extend up to ~60 Å above the OM. A plug loop implicated in iron uptake[12,13] is unusually long and protrudes ~25 Å above the cell surface.

Human Tf is a bilobal glycoprotein (~80 kDa) with a single ferric (Fe^{3+}) iron tightly bound within a cleft in each lobe (Fig. 1a and Supplementary Fig. S8). Each lobe of Tf consists of two subdomains which form the cleft: N1, N2, C1 and C2. In the absence of iron, each lobe adopts an open conformation (PDB code 2HAV)[14]. To best model Neisserial iron import, we solved the structure of diferric hTf at 2.1 Å resolution (Fig. 2d and Supplementary Fig. 8). In our diferric structure, each lobe is found in a fully closed conformation, nearly identical to the diferric structures for both porcine (PDB code 1H76) and rabbit (PDB code 1JNF) Tf.

When TbpA binds hTf, it sequesters ~2500 $Å^2$ of buried surface, with 81 TbpA residues and 67 hTf residues participating in the interaction (Fig. 1a, 1c, 1e, Supplementary Table 2). TbpA binds exclusively to the C-lobe of hTf, where electrostatic complementarity exists between the extracellular surface of TbpA (electropositive) and the C1-subdomain of hTf (electronegative) (Fig. 1b, 1d). Two striking features of the interface include: (1) the unusually long TbpA plug loop (residues 121–139) interacts directly with the C1-subdomain (Fig. 1a, 2a, 2c, Supplementary Fig. 5) and (2) an α-helix in TbpA extracellular loop 3 (residues 351–361, the L3 'helix finger') is inserted directly into the cleft of the C-lobe between the C1- and C2-subdomains (Fig. 1a, 2a, 2b, Supplementary Fig. 5). The interaction between TbpA and hTf was found to be relatively tolerant to point mutations in TbpA, as might be expected given the large binding interface (Supplementary Fig. 6).

The species specificity of Neisserial TbpA for hTf is an enigma. In *in vitro* assays, gonococcal and meningococcal TbpAs have been shown to bind human Tf, but not Tf from cow, horse, rabbit, mouse, rat, sheep, duck, or pig[15–17]. In addition, mice infected with *N. meningitidis* displayed a higher mortality rate when the iron source was Fe_2hTf rather than bovine Tf[18]. From the TbpA-hTf crystal structure, seven sites spanning both the C1- and C2-subdomains of hTf participate in binding TbpA (Fig. 1e, Supplementary Fig. 7), with each site containing one or more residues unique to human Tf.

Since TbpA shows limited sequence variation (Supplementary Fig. 5, Supplementary Table 4), is present in all clinical isolates, and nearly all the interactions with hTf are mediated by extracellular loops of TbpA, we attempted to disrupt the TbpA-hTf interface to see if this would be a viable therapeutic strategy. Peptides from four loops (loops 3, 7, 11, and the plug loop) that make substantial contacts with hTf were used as antigens for polyclonal antibody development (Supplementary Table 3). All four antibodies reduced hTf binding (Supplementary Fig. 9). These results show that although the TbpA-hTf interface is extensive, reagents can be designed to disrupt it.

TbpA induces a conformational change in the hTf C-lobe

In the full-length apo hTf structure[14], both the N- and C-lobes are in 'open' conformations, with 59.4° and 49.5° rotations required to align subdomains with diferric hTf (Fig. 2d, Supplementary Fig. 8). In the TbpA-hTf complex crystal structure, the N-lobe is in the fully

open conformation. Remarkably, interaction with TbpA causes the C-lobe to adopt a conformation midway between open and closed, with a 24° rotation required to align C1- and C2-subdomains with diferric hTf (Fig. 2d, Supplementary Fig. 10). The TbpA L3 helix finger is inserted into the cleft, where it interacts with D634 from the C1-subdomain and several residues from the C2-subdomain (Fig. 2a, b). The long TbpA plug loop also interacts with the surface of the C1-subdomain of hTf (Fig. 2c). These interactions induce a partial opening of the cleft in the hTf C-lobe, thereby destabilizing the iron coordination site to facilitate the release of iron from the C-lobe to TbpA. Figure 2e shows the residues coordinating iron in the hTf C-lobe structure and the significant increase in these distances when hTf binds TbpA. Such increases are clearly incompatible with tight binding of iron in the C-lobe.

X-ray and SAXS structures of TbpB and TbpB-(holo)hTf

Although only TbpA can acquire iron from hTf, the reaction is enhanced by expression of the co-receptor TbpB[7,8], which preferentially binds holo hTf[6]. To understand how TbpB facilitates iron extraction and uptake, we solved the structure of *N. meningitidis* TbpB (Fig. 3a, Supplementary Fig. 12,18, Supplementary Table 1). TbpB consists of N- and C-lobes that are structurally similar, sharing an 8-strand β-barrel subdomain flanked by a 4-strand 'handle' domain.

TbpBs from different isolates vary substantially in size and sequence (Supplementary Fig. 11), but the overall fold is conserved. Our structure aligns closely with three TbpB structures from porcine pathogens[19,20] and shows that sequence and conformational variations are found primarily in the N-lobe (Fig. 3a, Supplementary Fig. 12b). Specifically, residues affecting Tf binding lie on the distal surface of the N-lobe[19–22] and confer much of the Tf species specificity (Fig. 3a). We made point mutants at four sites on this surface that reduced or abolished binding to hTf (Fig. 3a, Supplementary Fig. 12). An analysis of our mutants and those reported previously demonstrates that the major site of interaction lies in the N-lobe.

To clarify the interactions of purified TbpA and TbpB with hTf, an ELISA was used to probe binding to Fe_2hTf, monoferric hTf with iron only in the N-lobe (Fe_N), or in the C-lobe (Fe_C), and apo hTf (incapable of binding iron in either lobe)[23]. Consistent with earlier studies using apo or holo hTf[6], TbpA binds all four hTfs with equal affinity regardless of the iron status of either lobe (Fig. 3b). In contrast, TbpB has a strong preference for hTf constructs with iron bound in the C-lobe, regardless of the coordination state of the N-lobe. These experiments clearly show that, at least *in vitro*, hTf interacts with TbpA and TbpB solely through the C-lobe and is not affected by the presence or absence of iron in the N-lobe. Our results indicate that *Neisseria* cannot utilize the entire serum Tf iron supply and that the primary function of TbpB is to select and concentrate on the cell surface only those forms of Tf that are able to provide iron to the bacterium.

Since TbpB primarily binds the C-lobe of hTf through its N-lobe, we performed steered molecular docking for the TbpB-hTf complex based on previous docking studies for the porcine complex[20] and on our mutagenesis results. We collected small angle X-ray scattering (SAXS) data on the TbpB-(holo)hTf complex (Supplementary Fig. 12, 13) and

used GASBOR[24] to construct the SAXS envelope (Fig. 3c, Supplementary Fig. 13). The resulting molecular envelope describes the spatial arrangement of TbpB and hTf, and was used to fit the TbpB-hTf complex structure. Binding TbpB to hTf buries ~1300 $Å^2$ of surface area and importantly, utilizes a region of the hTf C-lobe distinct from the site where TbpA binds (Fig. 5a).

Structure of the triple complex by single particle EM

Based on the TbpA-(apo)hTf crystal structure and the SAXS solution structure of the TbpB-(holo)hTf complex, we formed an *in silico* model for the TbpA-TbpB-(holo)hTf triple complex by superposing the two complexes along the C 1-subdomain of hTf (Fig. 4a). To test this model, we assembled the triple complex from its components (Fig. 4b) and visualized the resulting particles by negative staining electron microscopy (EM) (Fig. 4c and Supplementary Fig. 14). A set of 4240 particles was subjected to a reference-free classification in order to identify subsets of like images, representing molecules viewed in the same orientation; the members of each class were then averaged to suppress noise. Several of the class averages show a central density, ~45 Å across, to which two small globular densities are appended at points about 120° apart around its periphery (e.g. Fig. 4c asterisk, Supplementary Fig. 14). A plausible interpretation is that the central density corresponds to the β-barrel domain of TbpA and the two appended densities to TbpB and hTf (Supplementary Fig. 14), in agreement with our model for the triple complex.

Iron extraction and import

The X-ray, SAXS, and EM structures support a consistent arrangement for the TbpA-TbpB-(holo)hTf complex. While TbpA and TbpB each bind hTf tightly through the C-lobe, they have unique, non-overlapping binding sites (Fig. 5a). A consequence of the assembly of the triple complex is the formation of an enclosed chamber (volume of ~ 1000 $Å^3$) at the union of the three protein components, which sits directly above the plug domain of TbpA (Fig. 5b). This chamber may serve two important roles for iron acquisition by the bacteria: [1] prevent diffusion of iron released from hTf and [2] guide the iron toward the β-barrel domain of TbpA for subsequent transport.

A plausible mechanism for iron extraction from hTf is shown in Figure 5c. Insertion of the TbpA L3 helix finger into the cleft between the C1- and C2-subdomains of hTf positions a conserved lysine (TbpA K359, Supplementary Fig. 4) near the hTf triad of charged residues (hTf K534, R632, D634) that has been implicated in iron release from the C-lobe[25]. TbpA K359 is perfectly situated to interact with D634, which would disrupt the charge neutralization it normally provides to the two basic triad residues K534 and R632. This potential charge repulsion between the hTf C1-and C2-subdomains could induce cleft opening (as observed in the TbpA-(apo)hTf crystal structures) resulting in distortion of the C-lobe iron binding site and subsequent iron release. Significantly, a recent study indicates that an hTf D634A mutant has a rate of iron release that is 80-fold faster at pH 5.6 than the control under the same conditions[26].

To investigate iron transport across the OM, steered molecular dynamics (MD) was used to simulate interactions between TbpA and TonB (Supplementary Fig. 15). In the ground state

structure, a large, highly negative transmembrane cavity is located between the barrel wall and the plug domain, but access is restricted on the extracellular side by residues 91–96 (restriction loop) and on the periplasmic side by residues 65–71 (helical gate) from the plug domain (Fig. 5d). When force (designed to mimic interaction with TonB) is applied to the plug domain, it sequentially unfolds beginning with removal of the helical gate followed by the restriction loop, producing an unobstructed pathway from the extracellular space to the periplasm (Supplementary Movie 1). This pathway is lined by the EIEYE motif of the plug domain[13], which contains multiple oxygen donor groups that could transiently bind iron as it is transported through TbpA.

CONCLUSIONS

Humans and bacteria have each developed unique strategies to acquire iron from serum transferrin[27,28] (Supplementary Fig. 16). Our TbpA-TbpB-hTf X-ray, SAXS and EM structures suggest a mechanism for bacterial uptake of iron with the following characteristics: [1] a large TbpA-hTf binding interface with many human Tf-specific interactions, [2] iron removal from the hTf C-lobe by insertion of a helical element from TbpA into the iron binding cleft, and [3] iron transport across the outer membrane following TonB-dependent conformational changes in the TbpA plug domain. This system allows efficient extraction of iron despite the extremely high affinity of hTf bound iron at neutral pH. The TbpB co-receptor, which is tethered to the cell surface by a long, unstructured polypeptide chain, is able to attract and preferentially bind hTf with iron in the C-lobe, thereby increasing the efficiency of the system. Crucial to the mechanism, TbpA and TbpB associate with different regions of the hTf C-lobe, creating an enclosed chamber above the plug domain to ensure that iron is efficiently sequestered and directionally transported through the TbpA barrel (Supplementary Movie 2). Finally, since TbpA and TbpB are surface-exposed, antigenic, and required for Neisserial infections[29], our structures provide the necessary information for structure-based vaccine and drug design[30].

METHODS SUMMARY

The TbpA-(apo)hTf complex was crystallized from TbpA expressed in *E. coli* and (apo)hTf purchased from Sigma-Aldrich. For the TbpA-(apo)hTf C-lobe structure, hTf incorporating a protease cleavage site between N- and C-lobes was expressed in BHK cells and purified as described[31]. Full-length N-His tagged hTfs including holo, authentic apo, and both monoferric forms were expressed in BHK cells and purified as described.[23] The diferric hTf structure was solved using protein purchased from Sigma-Aldrich. The hTf C-lobe structure was solved using hTf C-lobe from a construct containing a TEV protease site between the N- and C-lobes, expressed in BHK cells, and purified[32]. TbpB was expressed in *E. coli*. X-ray data were collected at GM/CA and SER-CAT beamlines of the Advanced Photon Source synchrotron. SAXS data was collected on beamline BL4-2 at the Stanford Synchrotron Radiation Lightsource. EM data were collected on a CM120-LaB6 electron microscope (FEI), operating at 120kV. MD simulations were performed using the progam NAMD[33]. For more details see Methods.

METHODS

Cloning, expression and purification of TbpA

The *N. meningitidis* TbpA sequence from strain K454 (B15:P1.7,16) was subcloned into pET20b (Novagen) containing an N-terminal 10X-His tag. TbpA mutants were created using site-directed mutagenesis using QuikChange (Stratagene). For structural studies, mutation of M889 to Tyr improved expression levels. TbpA was expressed in BL21(DE3) cells at 20°C without induction in terrific broth (TB) and carbenicillin (carb). Expression for the mutants followed the same protocol.

For purification, cells were resuspended in lysis buffer (50 mM Tris-HCl, pH7.5, 200 mM NaCl, 1 mM $MgCl_2$, 10 μg /ml DNaseI, 100 μg/ml AEBSF) and lysed by two passages through an Emulsiflex C3 (Avestin) homogenizer at 4°C. The lysate was centrifuged at 12,000xg for 10 minutes remove unlysed cells and the supernatant was incubated with 2% Triton X-100 for 30 minutes at room temperature. The mixture was centrifuged at 160,000xg for 90 minutes at 4°C. The membrane pellets were resuspended in 50 mM Tris-HCl, pH7.5, 200 mM NaCl, 20 mM imidazole and solubilized by constant stirring using 5% Elugent for 16 hours at 4°C. Solubilized membranes were centrifuged at 265,000xg for 60 minutes at 4°C and the supernatant filtered and applied to a 15-ml Ni-NTA column. TbpA was eluted using 250 mM imidazole. Peak fractions were concentrated and applied to an S-300HR Sephacryl size exclusion column (GE Healthcare) using 20 mM Tris-HCl, pH7.5, 200 mM NaCl, 0.8% C_8E_4 and 0.02% NaN_3. Peak fractions were verified using SDS-PAGE and Western blot analysis using an anti-His monoclonal antibody (Sigma).

Cloning, expression and purification of TbpB

The TbpB sequence (starting at residue L22) from *N. meningitidis* K454 was codon optimized and synthesized by GenScriptand subsequently subcloned into a pET28b vector (Novagen). TbpB was expressed in T7-Express cells (NEB) at 37°C with IPTG induction at an OD_{600} of 0.75 – 1.0 with continued expression for four hours. Mutants were expressed using the same protocol.

For purification, cells were harvested and resuspended in 5ml PBS per gram of cell paste and supplemented with 10μg/ml AEBSF and 100μg/ml DNaseI. Cells were lysed by French press and then centrifuged for 45 minutes at 38,400xg. The supernatant was applied to a Ni-NTA column and washed with 10 column volumes of PBS. A final wash was performed with PBS containing 20mM imidazole before elution with PBS / 250 mM imidazole. Eluted protein was then dialyzed against PBS overnight at 4°C. For constructs where the His tag was removed, TEV-HIS protease was added, the sample was dialyzed and then passed through a second Ni-NTA column to remove uncleaved protein and protease. Finally, samples were purified by size exclusion chromatography in PBS / 0.02% NaN_3.

Crystallization and data collection

For crystallization of the TbpA-hTf complex, apo-human transferrin (Sigma) was mixed with TbpA at a 2:1 ratio and incubated on ice for 1 hour. The complex was isolated using Sephacryl S300HR chromatography equilibrated with 20 mM Tris-HCl, pH7.5, 200 mM

NaCl, 10 mM Na-citrate, 1 mM EDTA, 0.8% C_8E_4 (Anatrace) and 0.02% NaN_3. Fractions corresponding to the TbpA-hTF complex were verified using SDS-PAGE, pooled and concentrated to 10 mg/ml. Heptane-l,2,3-triol was added to 3% final concentration, incubated on ice for 30 minutes and then the protein sample was filtered prior to crystallization. Sparse matrix screening was performed using a TTP Labtech Mosquito crystallization robot using hanging drop vapor diffusion and plates incubated at 21°C. The best crystals were grown in 24 well Linbro plates (Hampton Research) from 20% Peg3350 and 200 mM $BaBr_2$. Data were collected at the SER-CAT beamline of the Advanced Photon Source of Argonne National Laboratory and data processed using HKL2000[34]. The space group was $P2_12_12_1$ with one mol/ASU and final cell parameters a=91.014, b=129.362, c=198.589, α=90.00, β=90.00, γ=90.00.

For crystallization of the TbpA-hTf C-lobe complex, hTf C-lobe[31] was mixed in a 2:1 ratio with TbpA and the complex isolated by Sephacryl S300HR chromatography using 20 mM Tris-HCl, pH7.5, 200 mM NaCl, 0.1% LDAO and 0.02% NaN_3. Final crystal conditions consisted of 21% PEG 1000, 100mM sodium acetate buffer (pH 4.8), 200mM NaCl, 0.1% LDAO and 3% heptane-1,2,3-triol. Data were collected and processed as described for the TbpA-hTf complex. The space group was P21 with one mol/ASU with final cell parameters a=58.055, b=107.592, c=130.721, α=90.00, β=94.48, γ=90.00.

TbpB was crystallized from a 10mg/ml solution with 2.0 M NaCl and 2.0 M ammonium sulfate. Data were collected at the GM/CA CAT beamline of the Advanced Photon Source of Argonne National Laboratory and data were processed using HKL2000[34]. The space group was P21 with two molecules per ASU with final cell parameters a=75.288, b=82.761, c=111.882, α=90.00, β=105.95, γ=90.00.

For diferric hTf crystallization, 100 mg of holo hTf (Sigma) was solubilized and further purified by Sephacryl S300HR chromatography using 20 mM Tris-HCl, pH7.5 and 200 mM NaCl. The protein was then concentrated to ~50mg/mL crystallized using 100mM HEPES, pH 7.5, 1.6 M ammonium sulfate, and 2% PEG 1000, with red-tinted crystals appearing only after several months and being extremely sensitive to even slight temperature changes. Drops containing the crystals were quickly hydrated with 3.4 M ammonium sulfate immediately prior to being flash cooled in liquid nitrogen and stored for data collection. Data were collected at the SER-CAT beamline of the Advanced Photon Source of Argonne National Laboratory and data were processed using HKL2000[34]. The space group is C2 with six molecules per ASU and final cell parameters a=254.53, b=173.00, c=150.15, α=90.00, β=123.26, γ=90.00.

For hTf C-lobe crystallization, (holo)C-lobe[32] was mixed with excess TbpB N-lobe and the complex isolated by size exclusion chromatography as above in in 25mM Tris pH8.0, 200mM NaCl. The complex was concentrated to ~10mg/ml and broad screening performed using a Mosquito crystallization robot. Several crystallization conditions were observed, however none were red in color as might be expected for iron bound crystals and most contained citrate, which is a known iron chelator. Data were collected and analyzed as for TbpB. The space group was I422 with one mol of hTf C-lobe/ASU with final cell

parameters a=95.847, b=95.847, c=204.140, α=90.00, β=90.00, γ=90.00. NO TbpB N-lobe was present in the crystals.

Structure determination

For TbpA-hTf, we were unable to collect useful heavy atom derivatives for experimental phasing and selenomethionine-substituted TbpA protein yields were not sufficient for crystallization. We eventually used molecular replacement in PHASER-CCP4[35] to solve the TbpA-hTF complex structure. Here, we first searched for each of the two domains (N-lobe and C-lobe) of hTF using the deposited coordinates (PDB code 2HAV), which produced good solutions with Z-scores above 8. However, while the electron density for the hTF molecule was reasonable, the electron density for TbpA was poor and could not be used for model building. Our attempts at using known TonB-dependent transporter structures as search models (barrel and plug, together and individually) were unsuccessful (low Z-scores and LLG scores). We then aligned the TbpA sequence to our structure-based sequence alignment reported in our recent review[4] and found that TbpA contained many conserved regions characteristic of TonB-dependent transporters. Using the alignment between TbpA and it closest relative, FhuA (10% identity, ClustalW), and trimming the extracelluar loops, 500 models within an RMSD of 5 Å were produced using Modeller (Accelrys). Each of these models was then used for molecular replacement within PHASER-CCP4[35], with two of them producing Z-scores above 8. The solution with the highest LLG (containing both hTF and the TbpA model) was refined in PHENIX[36] producing an initial R/Rfree of 0.43/0.48. Further model building was performed using COOT[37] and subsequent refinement done in PHENIX[36] and BUSTER-TNT[38]. During the final states of refinement, extra density was observed which was mapped to residues N413 and N611 of hTF, both of which are reported as possible N-linked glycosylation sites. Therefore, N-linked glycans were built for these two residues. The final structure was solved to 2.60 Å with R/Rfree values of 0.22/0.28. The TbpA-hTf C-lobe structure was solved by molecular replacement using the coordinates from the TbpA-hTF (full-length) structure reported here. Two search models were formed, one for TbpA and one for hTf C-lobe. PHASER-CCP4[35] was used for molecular replacement and subsequent refinement performed using PHENIX[36]. The structure was solved to 3.1 Å resolution wth final R/Rfree values of 0.24/0.29.

The TbpB structure was solved by molecular replacement using PDB code 3HOL. An initial model was created using the Swiss Model server[39] that was subsequently divided into four different search domains. PHASER-CCP4[35] was used for molecular replacement and subsequent refinement performed using PHENIX[36]. The structure was solved to 2.40 Å resolution with final R/Rfree values of 0.25/0.30.

The diferric hTf crystal structure was solved by molecular replacement using Phaser-CCP4[44]. Search models for the N-lobe and C-lobe were created separately with the program Chainsaw (CCP4) using the existing diferric porcine Tf coordinates (PDB code 1H76). Six copies of each lobe (6 molecules of hTf total) were found in the ASU and the iron sites were easily observed in the difference density. These iron sites were further verified in an anomalous difference electron density map. Refinement was performed using PHENIX[45] and the structure was solved to 2.1 Å resolution with final R/Rfree values of 0.19/0.23.

The non-glycosylated hTF-Clobe structure was solved by molecular replacement using PDB code 2HAU. An initial search model was formed by truncating the N-lobe domain. PHASER-CCP4[35] was used for molecular replacement and subsequent refinement performed using PHENIX[36]. The structure was solved to 1.7 Å resolution with final R/Rfree values of 0.17/0.19. For all structures, figures were made with PyMOL (Schrodinger) or Chimera[40] and annotated and finalized with Adobe Illustrator.

Dot blots

Whole cells (2μL, 0.01g/ml) and cell lysates (unmodified for TbpB samples, or incubated for 3 hours with 2mM EDTA and 1% DDM at room temperature for TbpA samples) were spotted onto nitrocellulose membrane and allowed to dry at room temperature. The membranes were then blocked with PBST 2% BSA for 15 minutes, washed and probed with HRP conjugated hTf (1:1000) (Jackson ImmunoResearch) for 15 minutes. The membrane was then washed and imaged using the colorimetric substrate 3,3'-diaminobenzidine (Sigma) where the appearance of a red dot indicated specific binding of the hTF-HRP conjugate. The results from the mutants were compared to wild type Tbp to determine their effect on hTF binding.

ELISA

Whole cells (100μL at 10 mg/ml or 1 mg/ml in PBS) of wild-type TbpA, empty vector control (pET20b), and TbpA mutants were added to a NUNC polystyrene 96-well plate (Fisher Scientific) and incubated at 37°C overnight. Wells were washed 2X with PBST and then blocked with PBST 2% BSA for 30 minutes and probed with hTf-HRP (1:1000) for 15 minutes. Wells were washed 2X in PBST, 2X in PBS, and then developed using 100 μL 3,3',5,5' - tetramethylbenzidine substrate (TMB, Sigma) for 5 minutes and terminated using Stop solution (Sigma). Absorbances of each well were determined using a BioRad iMark plate reader at 450nm and data normalized and compared to wild-type TbpA. Each experiment was performed in triplicate and data reported with standard errors.

Antibody blocking assays

Using the TbpA-hTf crystal structure reported here, we designed four different peptides based on four loops from TbpA (loops 3, 7,11, and plug loop) to be used as antigens for polyclonal antibody development (Precision Antibody). A fifth polyclonal antibody was developed using purified full length TbpA (1X PBS 7.4, 0.1% DDM). An ELISA was designed to probe whether or not these antibodies could block hTF binding. Here, TbpA-HIS (20ng) was incubated for 20 minutes in a final volume of 100 μL either alone or in the presence of each antibody (1:20) individually in PBS containing 0.05% Cymal-6 (Anatrace). In addition, we tested the antibodies that targeted TbpA loops in combinations to determine if an additive affect could be observed. Each sample was then transferred to a 96-well Ni-NTA Agarose HiSorb plate (Qiagen) and incubated for 30 minutes and washed 2X with PBST + 0.05% Cymal-6. Assays were performed as described in the previous section. In a second set of ELISAs, TbpA-HIS was first bound to the Ni-NTA Agarose HiSorb plate prior to incubation with antibodies. Results were analyzed and initial graphs made using Microsoft Excel. The graphs were then imported, annotated and finalized with Adobe Illustrator.

Protease accessiblity of TbpA and TbpA mutants

To confirm that TbpA and the TbpA mutants were being properly presented at the surface of the bacteria, we treated whole cells with trypsin (5 ug/mL final concentration) for 15 minutes at room temperature and the reaction was stopped by the addition of AEBSF (0.2 mg/ml final concentration). The cells were then centrifuged and supernatant removed. The pellets were then resuspended in LDS loading buffer, boiled for 10 minutes, centrifuged for 10 minutes, and then separated on a NuPAGE Novex 4–12% Bis-Tris gel. The samples were then transferred to a PVDF membrane using an iBlot system (Invitrogen) and Western blot analysis performed using a polyclonal anti-TbpA antibody (1:1000) and a monoclonal anti-HIS HRP conjugated antibody (Sigma) (1:5000). Here, each membrane was blocked with 2% BSA in 1X PBST for 15 minutes and then probed with either the anti-TbpA or anti-HIS HRP conjugated antibody for 30 minutes. The anti-TbpA membrane was then washed 2X with 2% BSA in 1X PBST and then probed with anti-Mouse HRP conjugated secondary antibodies for an additional 30 minutes. Both membranes were then washed 2X with 1X PBST, 2X with 1X PBS, and then imaged using the colorimetric substrate 3,3'-diaminobenzidine (Sigma). The results from the mutants were compared to wild type TbpA to determine which constructs were being presented on the surface of the cells.

Transferrin competition assays

To determine if the affinity of hTF to either TbpA or TbpB is affected by the conformation or coordination state of the N-lobe, we performed an ELISA competition assay using apo-hTF, holo-hTF, hTF-FeN (iron bound in N-lobe only), and hTF-FeC (iron bound in C-lobe only), which were expressed in BHK cells and purified as described[23]. Here, HIS-TbpA (20 ng) or HIS-TbpB (20 ng) was incubated for 15 minutes in a final volume of 100 uL in a 96-well Ni-NTA HiSorb plate (Qiagen) in 1X PBS (0.05% cymal-6 was added to all buffers for HIS-TbpA). Wells were washed 2X with PBST, blocked with 2% BSA in PBST for 15 minutes, and then incubated with each of the transferrin constructs (apo, holo, FeN, FeC) (100 ng each) for 15 minutes. Wells were washed again 2X with PBST, and then probed for 20 minutes with HRP conjugated hTF (1:1000) (Jackson ImmunoResearch) in 100 μL final volume. Wells were washed again 2X with PBST and then 2X with PBS and imaged using 100 μL 3,3',5,5' - tetramethylbenzidine substrate (Sigma) for ~5 minutes and terminated using Stop solution (Sigma). Data were collected and analyzed as described above.

Small angle X-ray scattering analysis

The TbpB-hTF complex was dialyzed overnight at 4°C into TBS, pH 7.4 (25 mM Tris, 137mM NaCl, 3mM KCl) and then filtered using a 0.2μm spin filter. Data were collected at concentrations of 1, 2.5, and 5 mg/ml at Stanford Synchrotron Radiation Lightsource beamline BL4-2. Data reduction and analysis were performed using the beamline software SAStool. The program AutoGNOM of the ATSAS suite[41] was used to generate P(r) curves and to the determine maximum dimension (Dmax) and radius of gyration (Rg) from the scattering intensity curve (I(q) versus q) in an automatic, unbiased manner, and rounds of manual fitting in GNOM[42] were used to verify these values. Ab initio molecular envelopes were computed by the programs GASBOR[24]. Ten iterations of GASBOR were averaged using DAMAVER[43]. Docking of the TbpB and diferric hTF crystal structures into the

molecular envelope was performed manually, guided by both previous docking studies[20] and mutagenesis results. Figures were made with PyMOL and annotated and finalized with Adobe Illustrator.

Modeling the TbpA-TbpB-hTF triple complex

The *in silico* TbpA-TbpB-hTF triple complex was assembled based on our crystal structures (TbpA-(apo)hTF, diferric hTf, TbpB) and SAXS analysis (TbpB-(holo)hTF) reported here. The crystal structure (TbpA-hTF) was aligned with our TbpB-hTF model using the C1-subdomain of hTF as a reference, yielding a triple complex containing a 1:1:1 ratio of TbpA, TbpB, and hTF. Figures were made with PyMOL and/or Maya (Autodesk) and annotated and finalized with Adobe Illustrator.

Electron microscopic analysis

The triple complex (TbpA-TbpB-(holo)hTF) was prepared from separately purified components by first forming a complex between TbpB and (holo)hTf which was purified by size exclusion chromatography in 1X PBS. Cymal-6 was added to a final concentration of 0.05% and purified TbpA (in 1X PBS, 0.05% Cymal 6) was added to the mixture using an excess of the TbpB-(holo)hTf complex. The triple complex (which retains a 1:1:1 stoichiometry) was isolated by sized exclusion chromatography in Buffer A (1X PBS in 0.05% Cymal 6) and used immediately for EM experiments. The complex was diluted with buffer A to an optimal concentration for EM (determined empirically to be ~1 μg/mL). Drops (4μL each) were applied to carbon coated, glow-discharged EM grids (EMS, USA). After 1 min, the grid was blotted, washed twice with Buffer A, once with distilled water, and then stained with 2% uranyl acetate. Grids were observed with a CM120 La-B6 electron microscope (FEI), operating at 120kV. Micrographs were recorded on SO163 film (Kodak) at a nominal magnification of 45,000, and digitized on a Nikon Coolscan 9000 at a rate corresponding to 1.55 Å/pixel. The large majority of particles distributed evenly on the grid and were essentially uniform in size (~ 90–110 Å in diameter), indicative of a homogeneous population.

The particles were variable in substructure, suggesting that the molecules deposit on the grid in a variety of orientations. Accordingly, a data set of 4240 particles was subjected to a "reference-free" classification, using SPIDER[58], EMAN[59], and Bsoft[60]. Images were picked uaing a box 256×256 pixel box, and binned 4 times (to 6.2Å/pixel) to increase the signal-to-noise ratio and the speed of calculation. Initial reference-free classification and averaging were performed using EMAN; then further classification was done in SPIDER, using principal component analysis (PCA) with 3 cycles of iteration. We chose to obtain 56 final class averages, based on a cluster distribution obtained from PCA.

The coordinates of the modeled triple complex were converted to a density map and low-pass filtered to 15 Å. The sampling rate of the density map was set to be same as the EM images and 2D projections were calculated at angular increments of 30° (Supplementary Fig. 14b). Comparisons and matching between the EM class averages and the model reprojections were done in terms of cross-correlation coefficients. A few ambiguous cases

were reassigned by visual assessment. Figures were made with Chimera and annotated and finalized with Adobe Illustrator.

Molecular dynamics simulations

For simulations of TbpA bound to (apo)hTf, a membrane-water system containing the protein complex was first built using VMD[44]. The complex was placed in a DMPE bilayer as used previously[45], with the barrel of TbpA aligned with the membrane's hydrophobic core, and then fully solvated. Disulfide bonds for three pairs in TbpA and 19 pairs in hTf were added based on S-S proximity. Ca^{2+} and Cl^- ions were added to a concentration of 100 mM, resulting in an initial size of 264,000 atoms. The system was equilibrated in stages for 13.5 ns, including 10 ns of fully unrestrained dynamics. The simulations were run using NAMD 2.7[33] in the NPT ensemble at a temperature of 310K and a pressure of 1 atm; after the first 3.5 ns of equilibration, the area of the membrane was fixed. Other simulation parameters were set identically to those used previously[45]. For steered MD (SMD) simulations, the Cα atom of the TbpA N-terminal plug domain residue was pulled in the -z direction, away from the membrane, at a constant velocity of 5 Å/ns[33,46]. To counterbalance the pulling forces, six residues at the extracellular periphery of the barrel domain were restrained in the z direction. An adaptive procedure was used to limit the maximum required system size during SMD simulations[47]. When the extension of the unfolded region of the plug domain brought it near the periodic boundary, the simulation was stopped, the unfolded region of the plug domain distant from the barrel and membrane was cleaved, and the simulation restarted after a short equilibration of the water with the new N-terminal residue being pulled. With this procedure, utilized three times, approximately 150 Å of pulling was accomplished while keeping the system sizes below 300,000 atoms.

Sequence analysis and alignments

Sequence analysis and alignments were performed and analyzed with the programs STRAP[48] and JalView[49]. Figures were annotated and finalized with Adobe Illustrator.

Supplementary Material

Refer to Web version on PubMed Central for supplementary material.

Acknowledgements

REFERENCES

1. Deasy A, Read RC. Challenges for development of meningococcal vaccines in infants and children. Expert Rev Vaccines. 2011; 10:335–343. [PubMed: 21434801]

2. CDC. Cephalosporin Susceptibility Among *Neisseria gonorrhoeae* Isolates --- United States, 2000--2010. Morbidity and Mortality Weekly Report. 2011; 60:873–877. [PubMed: 21734634]

3. Grifantini R, et al. Identification of iron-activated and -repressed Fur-dependent genes by transcriptome analysis of *Neisseria meningitidis* group B. Proc Natl Acad Sci U.S.A. 2003; 100:9542–9547. [PubMed: 12883001]

4. Noinaj N, Guillier M, Barnard TJ, Buchanan SK. TonB-dependent transporters: regulation, structure, and function. Annu Rev Microbiol. 2010; 64:43–60. [PubMed: 20420522]

5. Boulton IC, et al. Transferrin-binding protein B isolated from *Neisseria meningitidis* discriminates between apo and diferric human transferrin. Biochem J. 1998; 334:269–273. [PubMed: 9693129]

6. Krell T, et al. Insight into the structure and function of the transferrin receptor from *Neisseria meningitidis* using microcalorimetric techniques. The J Biol Chem. 2003; 278:14712–14722. [PubMed: 12571247]

7. Anderson JE, Sparling PF, Cornelissen CN. Gonococcal transferrin-binding protein 2 facilitates but is not essential for transferrin utilization. J Bacteriol. 1994; 176:3162–3170. [PubMed: 8195069]

8. Irwin SW, Averil N, Cheng CY, Schryvers AB. Preparation and analysis of isogenic mutants in the transferrin receptor protein genes, tbpA and tbpB, from *Neisseria meningitidis*. Mol Microbiol. 1993; 8:1125–1133. [PubMed: 8361357]

9. Rokbi B, et al. Evaluation of recombinant transferrin-binding protein B variants from *Neisseria meningitidis* for their ability to induce cross-reactive and bactericidal antibodies against a genetically diverse collection of serogroup B strains. Infect Immun. 1997; 65:55–63. [PubMed: 8975892]

10. Weynants VE, et al. Additive and synergistic bactericidal activity of antibodies directed against minor outer membrane proteins of Neisseria meningitidis. Infect Immun. 2007; 75:5434–5442. [PubMed: 17664268]

11. Price GA, Masri HP, Hollander AM, Russell MW, Cornelissen CN. Gonococcal transferrin binding protein chimeras induce bactericidal and growth inhibitory antibodies in mice. Vaccine. 2007; 25:7247–7260. [PubMed: 17720283]

12. Yost-Daljev MK, Cornelissen CN. Determination of surface-exposed, functional domains of gonococcal transferrin-binding protein A. Infect Immun. 2004; 72:1775–1785. [PubMed: 14977987]

13. Noto JM, Cornelissen CN. Identification of TbpA residues required for transferrin-iron utilization by *Neisseria gonorrhoeae*. Infect Immun. 2008; 76:1960–1969. [PubMed: 18347046]

14. Wally J, et al. The crystal structure of iron-free human serum transferrin provides insight into inter-lobe communication and receptor binding. J Biol Chem. 2006; 281:24934–24944. [PubMed: 16793765]

15. Cornelissen CN, Biswas GD, Sparling PF. Expression of gonococcal transferrin-binding protein 1 causes *Escherichia coli* to bind human transferrin. J Bacteriol. 1993; 175:2448–2450. [PubMed: 8468302]

16. Schryvers AB, Morris LJ. Identification and characterization of the transferrin receptor from *Neisseria meningitidis*. Mol Microbiol. 1988; 2:281–288. [PubMed: 3132585]

17. Stokes RH, Oakhill JS, Joannou CL, Gorringe AR, Evans RW. Meningococcal transferrin-binding proteins A and B show cooperation in their binding kinetics for human transferrin. Infect Immun. 2005; 73:944–952. [PubMed: 15664936]

18. Schryvers AB, Gonzalez GC. Comparison of the abilities of different protein sources of iron to enhance *Neisseria meningitidis* infection in mice. Infect Immun. 1989; 57:2425–2429. [PubMed: 2545624]

19. Calmettes C, et al. Structural variations within the transferrin binding site on transferrin-binding protein B, TbpB. J Biol Chem. 2011; 286:12683–12692. [PubMed: 21297163]

20. Moraes TF, Yu RH, Strynadka NC, Schryvers AB. Insights into the bacterial transferrin receptor: the structure of transferrin-binding protein B from *Actinobacillus pleuropneumoniae*. Mol Cell. 2009; 35:523–533. [PubMed: 19716795]

21. Cornelissen CN, Anderson JE, Sparling PF. Characterization of the diversity and the transferrin-binding domain of gonococcal transferrin-binding protein 2. Infect Immun. 1997; 65:822–828. [PubMed: 9009351]

22. Silva LP, et al. Conserved interaction between transferrin and transferrin-binding proteins from porcine pathogens. J Biol Chem. 2011; 286:21353–21360. [PubMed: 21487007]

23. Mason AB, et al. Expression, purification, and characterization of authentic monoferric and apo-human serum transferrins. Protein Expr Purif. 2004; 36:318–326. [PubMed: 15249056]

24. Svergun DI, Petoukhov MV, Koch MH. Determination of domain structure of proteins from X-ray solution scattering. Biophys J. 2001; 80:2946–2953. [PubMed: 11371467]

25. Halbrooks PJ, et al. Investigation of the mechanism of iron release from the C-lobe of human serum transferrin: mutational analysis of the role of a pH sensitive triad. Biochemistry. 2003; 42:3701–3707. [PubMed: 12667060]

26. Steere AN, Byrne SL, Chasteen ND, Mason AB. Kinetics of iron release from transferrin bound to the transferrin receptor at endosomal pH. Biochim Biophys Acta. 2011

27. Cheng Y, Zak O, Aisen P, Harrison SC, Walz T. Structure of the human transferrin receptor-transferrin complex. Cell. 2004; 116:565–576. [PubMed: 14980223]

28. Eckenroth BE, Steere AN, Chasteen ND, Everse SJ, Mason AB. How the binding of human transferrin primes the transferrin receptor potentiating iron release at endosomal pH. Proc Natl Acad Sci U.S.A. 2011; 108:13089–13094. [PubMed: 21788477]

29. Hobbs MM, et al. Experimental Gonococcal Infection in Male Volunteers: Cumulative Experience with *Neisseria gonorrhoeae* Strains FA1090 and MS11mkC. Front Microbiol. 2011; 2:123. [PubMed: 21734909]

30. Scarselli M, et al. Rational design of a meningococcal antigen inducing broad protective immunity. Sci Transl Med. 2011; 3:91ra62.

31. Zak O, Aisen P. A new method for obtaining human transferrin C-lobe in the native conformation: preparation and properties. Biochemistry. 2002; 41:1647–1653. [PubMed: 11814359]

32. Steere AN, et al. Properties of a homogeneous C-lobe prepared by introduction of a TEV cleavage site between the lobes of human transferrin. Protein Expr Purif. 2010; 72:32–41. [PubMed: 20064616]

33. Phillips JC, et al. Scalable molecular dynamics with NAMD. J Comput Chem. 2005; 26:1781–1802. [PubMed: 16222654]

34. Otwinowski Z, Minor W. Processing of X-ray data collected in oscillation mode. Meth Enzymol. 1997; 276:307–326.

35. McCoy AJ, et al. Phaser crystallographic software. J Appl Crystallogr. 2007; 40:658–674. [PubMed: 19461840]

36. Adams PD, et al. PHENIX: building new software for automated crystallographic structure determination. Acta Crystallogr D Biol Crystallogr. 2002; 58:1948–1954. [PubMed: 12393927]

37. Emsley P, Cowtan K. Coot: model-building tools for molecular graphics. Acta Crystallogr D Biol Crystallogr. 2004; 60:2126–2132. [PubMed: 15572765]

38. Blanc E, et al. Refinement of severely incomplete structures with maximum likelihood in BUSTER-TNT. Acta Crystallogr D Biol Crystallogr. 2004; 60:2210–2221. [PubMed: 15572774]

39. Arnold K, Bordoli L, Kopp J, Schwede T. The SWISS-MODEL workspace: a web-based environment for protein structure homology modelling. Bioinformatics. 2006; 22:195–201. [PubMed: 16301204]

40. Pettersen EF, et al. UCSF Chimera--a visualization system for exploratory research and analysis. J Comput Chem. 2004; 25:1605–1612. [PubMed: 15264254]

41. Petoukhov MV, Svergun DI. Analysis of X-ray and neutron scattering from biomacromolecular solutions. Curr Opin Struct Biol. 2007; 17:562–571. [PubMed: 17714935]

42. Svergun O, Genkina OA. [The dependence of the dynamics of the extinction of a temporary connection on the recognizability of a reinforcing stimulus]. Zh Vyssh Nerv Deiat Im I P Pavlova. 1991; 41:700–707. [PubMed: 1660650]

43. Volkov VV, Svergun DI. Uniqueness of ab initio shape determination in small-angle scattering. J. Appl. Crystallogr. 2003; 36:860–864.

44. Humphrey W, Dalke A, Schulten K. VMD: visual molecular dynamics. J Mol Graph. 1996; 14:33–38. [PubMed: 8744570]

45. Gumbart J, Wiener MC, Tajkhorshid E. Coupling of calcium and substrate binding through loop alignment in the outer-membrane transporter BtuB. J Mol Biol. 2009; 393:1129–1142. [PubMed: 19747487]

46. Sotomayor M, Schulten K. Single-molecule experiments in vitro and in silico. Science. 2007; 316:1144–1148. [PubMed: 17525328]

47. Gumbart J, Wiener MC, Tajkhorshid E. Mechanics of force propagation in TonB-dependent outer membrane transport. Biophys J. 2007; 93:496–504. [PubMed: 17449669]

48. Gille C, Frommel C. STRAP: editor for STRuctural Alignments of Proteins. Bioinformatics. 2001; 17:377–378. [PubMed: 11301311]

49. Waterhouse AM, Procter JB, Martin DM, Clamp M, Barton GJ. Jalview Version 2--a multiple sequence alignment editor and analysis workbench. Bioinformatics. 2009; 25:1189–1191. [PubMed: 19151095]
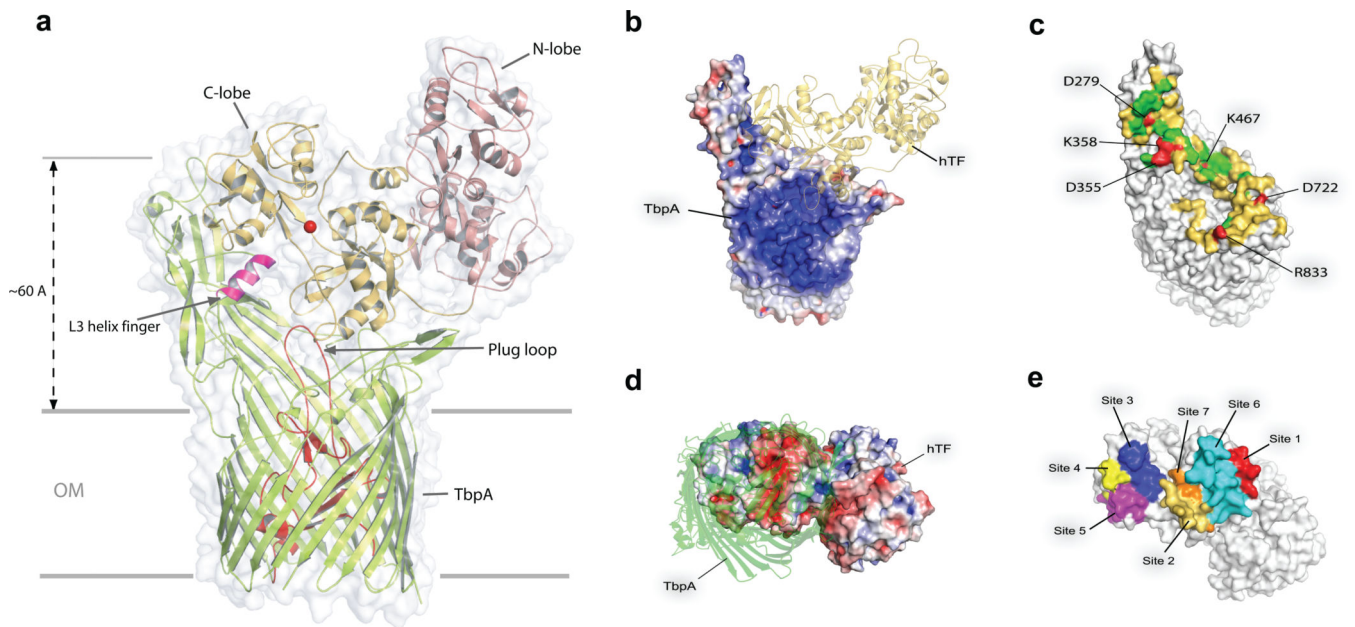
Figure 1. Crystal structure of the TbpA-(apo)hTF complex
a, The TbpA beta barrel is lime, the plug is red, the helix finger is magenta. For hTf, the C-lobe is gold and the N-lobe is salmon. A ferric ion has been modeled into the C-lobe as a red sphere. **b,** Electrostatic potential of TbpA viewed from the extracellular surface with hTf shown in gold ribbon. **c,** Residues of TbpA that bind hTf: gold, hydrophobic interactions; green, hydrogen bonds; red, salt bridges (residues labeled). **d,** Electrostatic potential of hTf viewed from the extracellular surface with TbpA shown in green ribbon. **e,** Surface representation of hTf showing regions that bind TbpA.
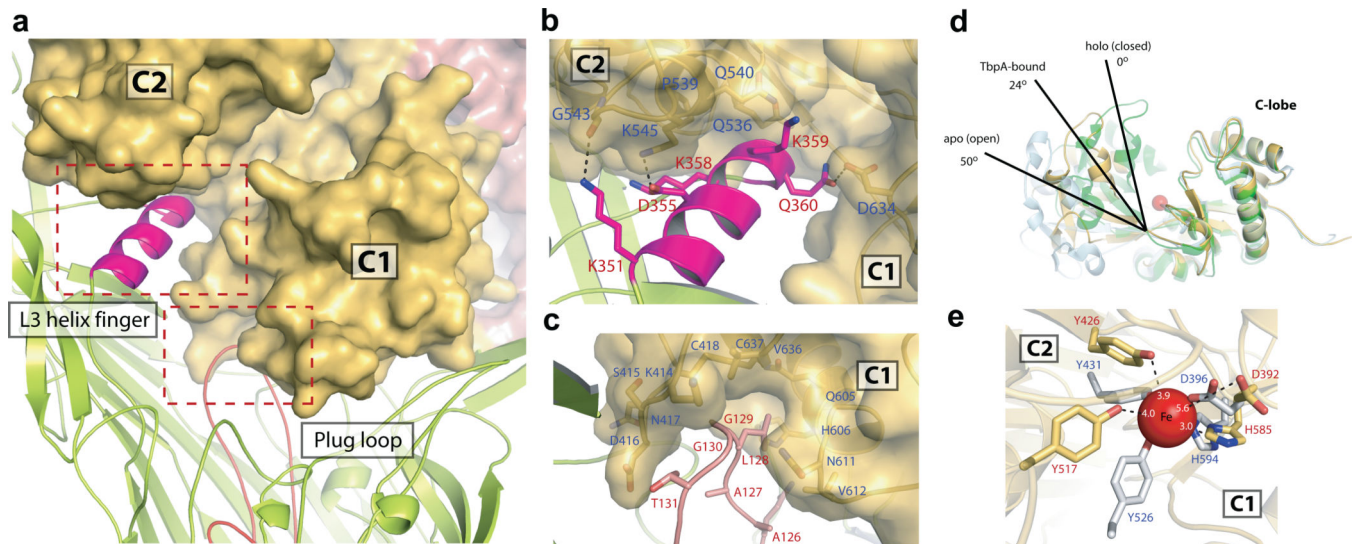
Figure 2. TbpA distorts the iron coordination site in the hTf C-lobe by inserting a helix from extracellular loop three

a, TbpA (green) inserts a helix finger from extracellular loop 3 (magenta) into the cleft of the hTf C-lobe (gold). **b,** The helix finger interacts with the hTf C-lobe residues through mainchain and sidechain interactions. **c,** The long TbpA plug loop (pink) interacts with residues from the C1 subdomain. **d,** Comparison of C-lobe conformations for holo (green), apo (gray, PDB code 2HAU), and TbpA-bound Tf (gold). **e,** Superposition of residues coordinating iron in diferric hTf (gray) with the same residues in hTf when bound to TbpA (gold). Distances for the residues coordinating iron are shown for the TbpA-bound state.
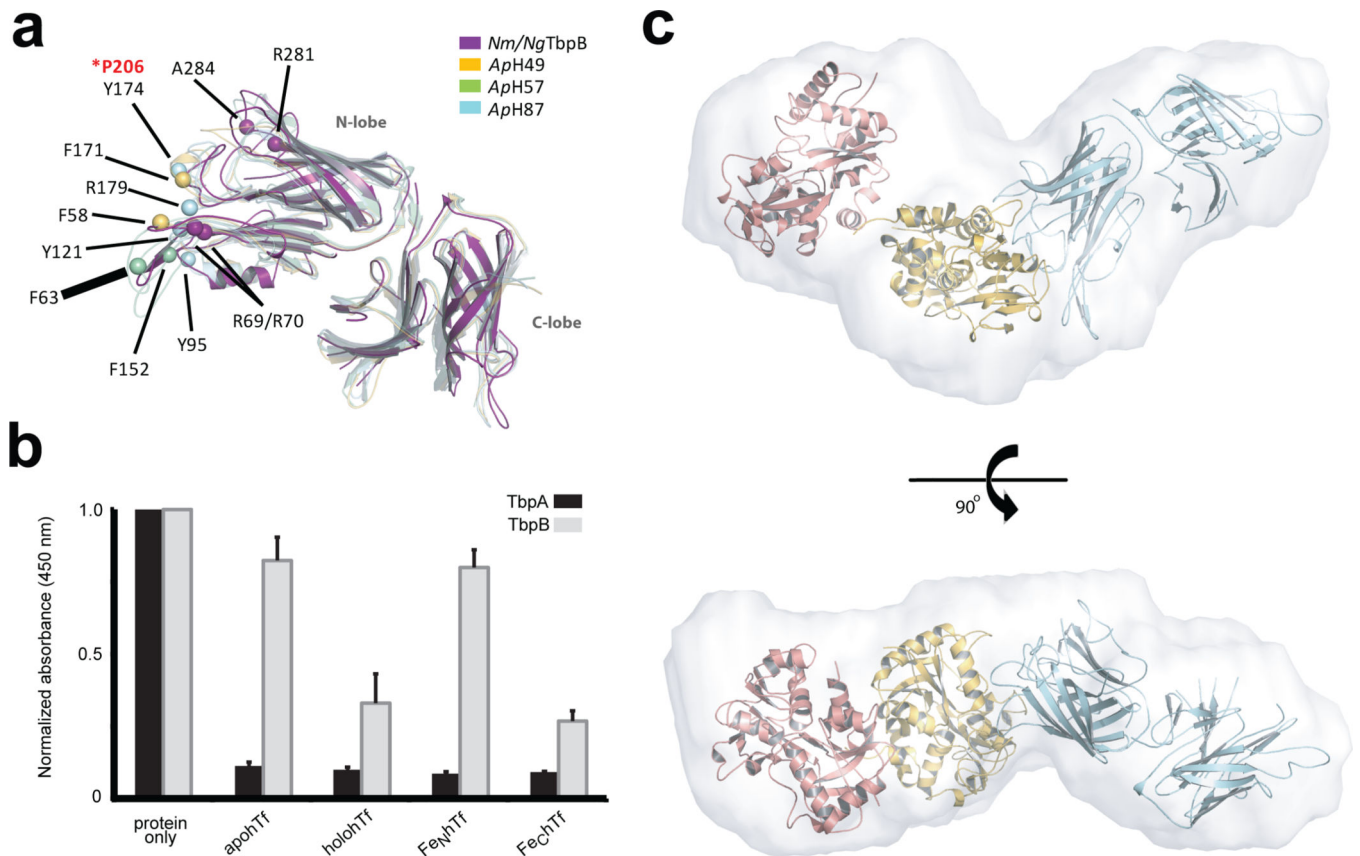
Figure 3. SAXS analysis of the *N. meningitidis* TbpB-(holo)hTf complex
a, Superposition of TbpB from *N. meningitidis* with three TbpB structures from porcine
pathogens. While C-lobes align closely, the N-lobes show sequence and structural
variability. Residues that diminish hTf binding when mutated are shown as spheres. Position
206 (proline in *N. meningitidis)* is critical for interaction with hTf. **b,** Competition ELISA
showing relative binding affinities of TbpA and TbpB for apo hTf, holo hTf, hTf-Fe$_N$, and
hTf-Fe$_C$. **c,** Fitting of the TbpB-(holo)hTf complex model into the averaged *ab initio*
envelope was performed using Chimera. TbpB is shown in cyan, hTf is shown in salmon (N-
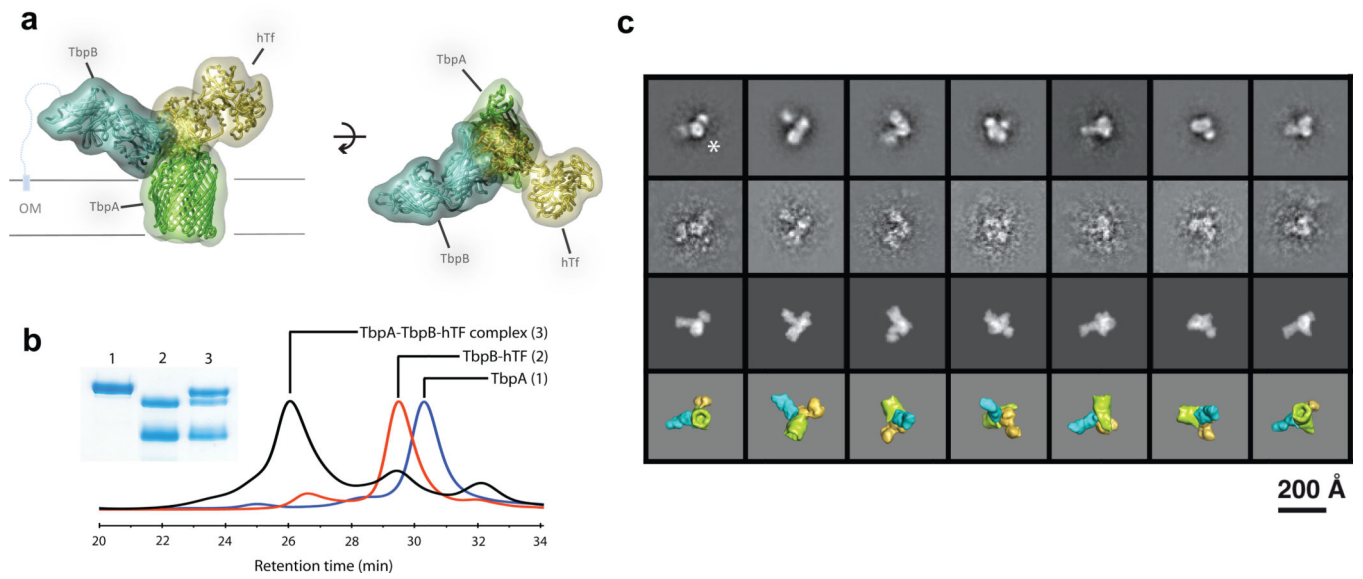lobe) and gold (C-lobe).

Figure 4. Analysis of the TbpA-TbpB-(holo)hTf triple complex by negative stain electron microscopy

a, Model of the triple complex. TbpA is green, TbpB is light blue, and hTf is gold. **b,** Purification of the triple complex by size exclusion chromatography. The Coomassie-stained SDS gel shows purified TbpA in lane 1, the TbpB-(holo)hTf complex in lane 2, and the TbpA-TbpB-(holo)hTf complex in lane 3. **c,** Row 1: set of seven non-redundant class averages of negatively stained complexes. Row 2: examples of individual images assigned to the respective classes. Row 3: reprojections of the model in the corresponding orientations, band-limited to 15Å resolution; Row 4: surface renderings of the band-limited model in the corresponding orientations.
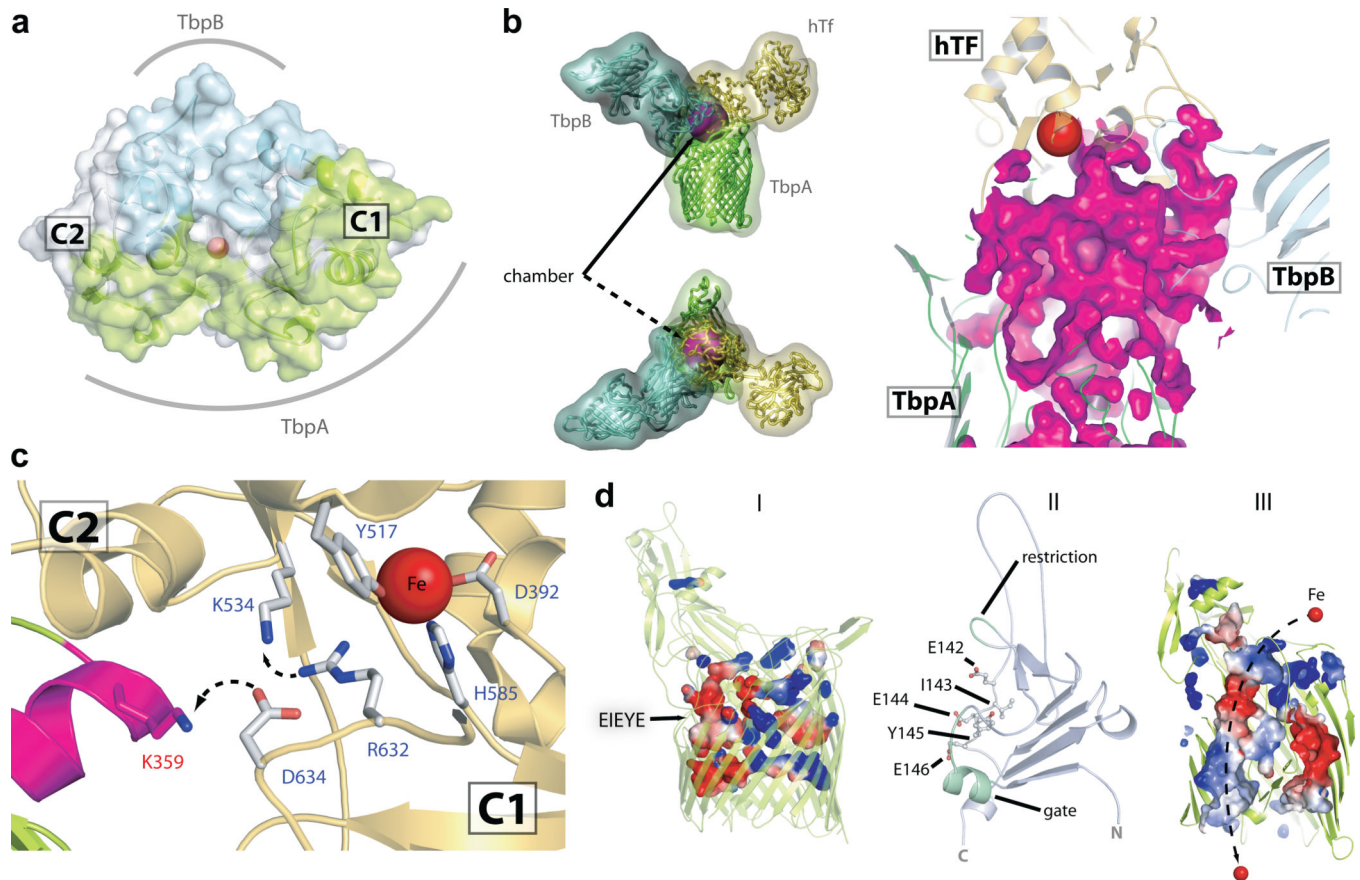
Figure 5. Mechanism for iron import
a, Binding surfaces of TbpA (green) and TbpB (cyan) mapped onto the hTF C-lobe. **b,** Enclosed chamber formed by TbpA-TbpB-(holo)hTF *(left,* magenta sphere). A cutaway view *(right)* from inside the chamber illustrates the proximity of the iron (red). **c,** Model for iron release. Conserved K359 in the L3 helix finger is positioned to interact with residues that regulate iron release in eukaryotic iron uptake. **d,** Import of iron through TbpA. (I) An electrostatic surface depicts cavities between the TbpA barrel and plug domain. (II) Plug domain constrictions close the tunnel. (III) MD simulations show removal of constrictions upon interaction with TonB.